Sawtooth relaxation oscillations, nonlinear helical flows and steady-state m/n=1 magnetic islands in low-viscosity tokamak plasma simulations

(Article begins on next page)

20 April 2024

Sawtooth relaxation oscillations, nonlinear helical flows and steady-state <i>m/n</i>=1 magnetic islands in low-viscosity tokamak plasma simulations

1   **Sawtooth relaxation oscillations, nonlinear helical flows and steady-state *m/n*=1**

2   **magnetic islands in low-viscosity tokamak plasma simulations.**

3   W. Zhang[1], Z. W. Ma[1,a)], F. Porcelli[2], H. W. Zhang[1], and X. Wang[1]

4   [1]Institute for Fusion Theory and Simulation, Department of Physics, Zhejiang

5   University, Hangzhou 310027, China

6   [2]Department of Applied Science and Technology, Polytechnic University of Turin,

7   Turin, Italy

8

9   **Abstract**

10   A numerical study on the influence of plasma viscosity and of the plasma β

11   (=kinetic pressure/magnetic pressure) parameter on the nonlinear evolution of

12   resistive internal kink modes in tokamak plasmas is presented. A new regime with

13   relatively low viscosity is found, such that sawtooth oscillations spontaneously evolve

14   towards states with stationary *m/n*=1 magnetic islands. It is suggested that the

15   mechanism at work in the limit of small viscosity is related to magnetic flux pumping,

16   which, allied with the nonlinear resistive internal kink dynamics, leads to a stationary

17   helical flow, only weakly dissipated by viscosity and entirely self-consistent with the

18   presence of saturated *m/n*=1 stationary magnetic islands. It is also found that the

19   threshold viscosity value for the onset of the steady state regime increases with

20   increasing β values. The newly found regime for a steady-state *m/n*=1 magnetic

21   island may be relevant for the understanding of tokamak experiments, where saturated

22   helical structures such as the density snake and steady-state magnetic islands are

23   sometimes observed in the core plasma region where the safety factor is close to or

24   below unity.

25   [a)] Corresponding Author: zwma@zju.edu.cn

I.   Introduction

Sawtooth relaxation oscillations, or simply *sawteeth*, are commonly observed in Tokamak fusion devices. A sawtooth consist of a slow ramp, during which the plasma temperature, density and current density profiles peak in the core region, and a rapid relaxation, also called the sawtooth crash, during which the temperature, density and current density profiles are rapidly flattened. Sawteeth occur whenever the central safety factor, q, approaches or falls below unity in the plasma core [1-9].

There are different kinds of sawtooth oscillations; among them, normal sawteeth, [1, 7] small sawteeth, [8] and compound sawteeth [9]. Normal sawteeth are dangerous for Tokamak operations, since not only they flatten the plasma temperature, but they can also trigger neo-classical tearing modes in nearby resonant surfaces [10-12], leading to significant energy confinement degradation. On the other hand, small sawteeth are less likely to trigger neo-classical tearing modes [13], therefore the confinement degradation they cause is tolerable for the performance of a fusion reactor [14]. Furthermore, small sawteeth may help preventing impurity and fusion ash accumulation in the core plasma region. Consequently, small sawteeth are the preferred scenario for future fusion reactor experiments such as ITER [15].

Auxiliary heating systems, such as ion cyclotron resonance heating (ICRH), neutral beam injection (NBI), electron cyclotron resonance heating (ECRH), and lower hybrid current drive (LHCD) [6, 16-25] can be used to control the sawtooth dynamics and achieve the small sawtooth regime. However, the question arises as to whether the plasma may "spontaneously" evolve towards self-organized states, where sawtooth activity is totally absent [26, 27], or, alternatively, where a remnant magnetic island with toroidal and dominant poloidal mode numbers $n=m=1$ caused by the sawtooth dynamics itself reaches a stationary state [28].

From a theoretical point of view, it is widely accepted that sawtooth oscillations are triggered by the instability of a resistive internal kink mode with mode numbers $n=m=1$ and that the trigger conditions for the onset of this mode may be strongly affected by two-fluid effects such as electron and ion diamagnetism [29-35]. Weakly collisional or collisionless effects may also be important (see, e.g., Ref. [34, 35] and

other references cited therein).

Less well-understood are the nonlinear consequences of the internal kink instability. According to the standard "complete reconnection model" proposed by Kadomtsev in 1975 [29], a $m/n=1$ magnetic island starts growing at the top of the sawtooth ramp and rapidly fills the entire core plasma region where the safety factor is below unity, up to the so-called mixing radius (which can be evaluated theoretically using conservation of helical flux). As a consequence, the safety factor goes back to above unity in the plasma core and poloidal symmetry of the magnetic structure is restored rapidly after the sawtooth crash. In other words, according to Kadomtsev's model, the presence of the $m/n=1$ magnetic island is limited to short time periods immediately before and after the sawtooth crash, while the much longer sawtooth ramps are basically island-free.

While Kadomstev theory is sometimes corroborated by experimental observations [1], there are several examples from tokamak experiments where the plasma is observed to behave in a different way. For instance, in the experiments discussed in Refs. [5, 8], the $m/n=1$ magnetic island is observed to persist for long periods of time during sawtooth ramps, e.g. in the form of successor $m/n=1$ oscillations, and the central safety factor is observed to stay below unity after the sawtooth crash. This situation has prompted the formulation of a semi-heuristic "incomplete reconnection model", a discussion of which can be found, for instance, in Ref. [30]. Even more challenging is the interpretation of the so-called snake phenomenon observed in tokamak plasmas [36-38]. A snake is basically a relatively high plasma density helical structure, likely associated with a nearly-stationary $m=n=1$ magnetic island, co-existing with sawtooth relaxation oscillations.

In view of the importance of sawtooth control in tokamak fusion experiments, the mechanism for the onset of stationary $m/n=1$ magnetic island scenario is worth further investigations and it is the objective of this article. As is well known, two-fluid diamagnetic effects in specific plasma regimes do affect importantly the nonlinear dynamics of sawtooth oscillations.[31, 39-41] However, in this manuscript and as a

research strategy, we would like to draw attention to the existence of a new, low viscosity regime, and therefore we select regimes where diamagnetic effects are shown in our simulations to play a negligible role of the existence of a saturated $m/n=1$ island state at low viscosity. More central to our analysis is the nonlinear evolution of the helical plasma flow induced by the internal kink magnetic reconnection process. In a recent article by Shen and Porcelli [28], it was shown that in the limit of very high viscosity the nonlinear sawtooth dynamics indeed tends to evolve towards a stationary state. This regime, however, requires unrealistically large values of viscosity, i.e., values of the relevant magnetic Prandtl number $V = \nu / \eta$ approaching 10^3. The main objective of this article is therefore to investigate the behavior of $m/n=1$ magnetic island for more realistic viscosity values.

The main result of our analysis is that sawtooth oscillations may spontaneously evolve into states with stationary $m/n=1$ magnetic island also in the limit of very small viscosity. Somehow, the analysis of Ref. [28] totally missed this result. Clearly, the mechanism at work for the self-sustainment of the $m/n=1$ magnetic island in the presence of nonlinear helical flows is different from the one conjectured in Ref. [28]. Most likely, the mechanism at work in the limit of small viscosity is more akin to the magnetic flux pumping concept first discussed in Refs. [42, 43]. However, while in recent works[27, 44] the flux pumping mechanism maintains the q profile close to and above unity, thus preventing the onset of resistive internal kink modes leading to magnetic reconnection and the formation of $m/n=1$ magnetic islands, in our case flux pumping allied with the nonlinear resistive internal kink dynamics leads to a stationary helical flow, only weakly dissipated by viscosity, which is entirely self-consistent with the presence of the stationary magnetic island.

In order to focus on the nonlinear flow dynamics associated with the resistive internal kink mode, we have used the code CLT, whose features are discussed in more details in the next section. The CLT code was used in the past to study two-fluid and extended-MHD effects on the nonlinear magnetic reconnection dynamics [33, 45]. In

4 / 30

this article, where two-fluid and extended-MHD effects are beyond the scope of the present study, we shall perform viscosity scans at fixed electrical resistivity, with the viscosity coefficient varied by three orders of magnitude. In addition, we shall discuss the results of simulations at different values of the dimensionless β-parameter (β = plasma kinetic pressure/magnetic pressure). Since the drive for the internal kink instability is stronger at larger β, it is perhaps not surprising that the kinetic energy of the nonlinear helical flow turns out to be larger at larger β values at fixed values of resistivity and viscosity. Consequently, β affects the ability to achieve nonlinear stationary states with magnetic islands.

II. Model description

CLT is a three-dimensional toroidal Hall-MHD code. In dimensionless units, the equations used in CLT [46] are given as follows:

$$\frac{\partial \rho}{\partial t} = -\nabla \cdot (\rho \mathbf{v}) + \nabla \cdot [D\nabla(\rho)], \tag{1}$$

$$\frac{\partial p}{\partial t} = -\mathbf{v} \cdot \nabla p - \Gamma p \nabla \cdot \mathbf{v} + \nabla \cdot [\kappa_\perp \nabla(p - p_0)] + \nabla \cdot [\kappa_\parallel \nabla_\parallel p], \tag{2}$$

$$\frac{\partial \mathbf{v}}{\partial t} = -\mathbf{v} \cdot \nabla \mathbf{v} + (\mathbf{J} \times \mathbf{B} - \nabla p) / \rho + \nabla \cdot [\nu \nabla(\mathbf{v})], \tag{3}$$

$$\frac{\partial \mathbf{B}}{\partial t} = -\nabla \times \mathbf{E}, \tag{4}$$

$$\mathbf{E} = -\mathbf{v} \times \mathbf{B} + \eta(\mathbf{J} - \mathbf{J}_0) + \frac{d_i}{\rho}(\mathbf{J} \times \mathbf{B} - \nabla p_e), \tag{5}$$

$$\mathbf{J} = \nabla \times \mathbf{B}, \tag{6}$$

where p_0 and $\mathbf{J}_0$ are the initial plasma pressure and current density, respectively, ρ, p_e, p, $\mathbf{v}$, $\mathbf{B}$, $\mathbf{E}$, and $\mathbf{J}$ are the plasma density, the electron pressure, the plasma pressure, the fluid velocity, the magnetic field, the electric field, and the current density, respectively. $\Gamma(= 5/3)$ is the ratio of specific heats. η, D, $\kappa_\perp$, $\kappa_\parallel$, and ν are the resistivity, the diffusion coefficient, the perpendicular and parallel thermal conductivity, and the viscosity, respectively. $d_i = c/\omega_{pi}$ is the ion inertial length,

with ω_{pi} the ion plasma frequency. It should be noted that the last term on the right side of Eq. (5) is the Hall term, which is associated with two-fluids effects. In Hall MHD, the ion temperature is assumed to be zero, i.e., $p = p_e$. As shown in our previous studies, the two-fluids effect is self-consistently included in the Hall-MHD equations, i. e. the ion-sound Larmor radius $\rho_s = d_i \sqrt{\mu_0 p / B_0^2}$ and the electron diamagnetic frequency $\omega_{*e} = -\dfrac{d_i m}{\rho r B} \dfrac{dp_e}{dr}$.

All the variables are normalized as follows: $\mathbf{B}/B_{00} \to \mathbf{B}$, $\mathbf{x}/a \to \mathbf{x}$, $\rho/\rho_{00} \to \rho$, $\mathbf{v}/v_A \to \mathbf{v}$, $t/t_A \to t$, $p/(B_{00}^2/\mu_0) \to p$, $\mathbf{J}/(B_{00}/\mu_0 a) \to \mathbf{J}$, $\mathbf{E}/(v_A B_{00}) \to \mathbf{E}$, $\eta/(\mu_0 a^2/t_A) \to \eta$, $D/(a^2/t_A) \to D$, $\kappa_\perp/(a^2/t_A) \to \kappa_\perp$, $\kappa_{\Box}/(a^2/t_A) \to \kappa_{\Box}$, $\nu/(a^2/t_A) \to \nu$, and $d_i/a \to d_i$, respectively. Here, B_{00} and ρ_{00} are the initial magnetic field and plasma density at the magnetic axis, respectively, a is the minor radius, $v_A = B_{00}/\sqrt{\mu_0 \rho_{00}}$ is the Alfvén speed, and $t_A = a/v_A$ is the Alfvén time.

Particular attention should be given to the term $\eta(\mathbf{J} - \mathbf{J}_0)$ in Eq. (5). The $-\eta \mathbf{J_0}$ part of this term is a source, which acts as magnetic pump [26] and serves the purpose of recovering the magnetic flux after each sawtooth crash. In other words, it is thanks to this term that the q profile is allowed to evolve after each sawtooth crash, eventually returning below unity and causing the next sawtooth crash to be triggered. We may also think of this source term as providing a sort of the magnetic pump.

Different from the original Hall-MHD equations, $\mathbf{E}$ is used as an intermediate variable in CLT, which could help to keep $\nabla \Box \mathbf{B} = 0$ during the simulations. When solving Eq. (1)-(6), the 4th order finite difference method is applied to derive the spatial derivatives, and the 4th order Runge–Kutta scheme is used to calculate the time integration. Since the physical boundary is not located at the grids, the cut-cell method is used to handle the boundary problems [47]. In the present manuscript, the fix boundary condition is used for all the variables. The convergence of the code has been ensured by varying space and time resolutions. In the present paper, the grids are

1
2
3
4
5
6
7
8
9
10
11
12
13
14
15
16
17
18
19
20
21
22
23
24
25
26
27
28
29
30
31
32
33
34
35
36
37
38
39
40
41
42
43
44
45
46
47
48
49
50
51
52
53
54
55
56
57
58
59
60

$256 \times 32 \times 256$ (R, ϕ, Z), and the spatial resolution is $1/128$ in R and Z.

III. Simulation results

A. Sawtooth oscillations with High β

The strategy for our simulations is as follows. The initial equilibrium is obtained from the NOVA code [48]. Mimicking a toroidal Tokamak configuration, the aspect ratio is chosen to be $R_0 / a = 4/1$. The initial q and pressure profiles are shown in Figure 1. With q on axis below unity, the most unstable mode is the $m/n=1/1$ resistive kink mode. In this subsection, the value of beta is fixed to be relatively high, $\beta \sim 3.8\%$. In order to investigate how viscosity plays a role in sawtooth dynamics at relatively high plasma beta, we carry out simulations at different values of the viscosity coefficient: $\nu=1.0 \times 10^{-3}$, $\nu=1.0 \times 10^{-4}$, $\nu=2.0 \times 10^{-5}$, and $\nu=6.0 \times 10^{-6}$. The electrical resistivity is fixed at the value $\eta = 2.5 \times 10^{-6}$. We agree that a constant resistivity model in our manuscript would be a limitation in regimes where diamagnetic as well as thermal conductivity effects are important, but, as we have already indicated in the introduction, as a research strategy we select parameter regimes where these effects are not affecting importantly the dynamics of the sawtooth dynamics at low viscosity. Other parameters are chosen to be $D = 1.0 \times 10^{-4}$, $\kappa_\perp = 2.0 \times 10^{-5}$, $\kappa_\parallel = 5 \times 10^{-2}$. We also switch off Hall/diamagnetic effects by choosing $d_i = 0$.
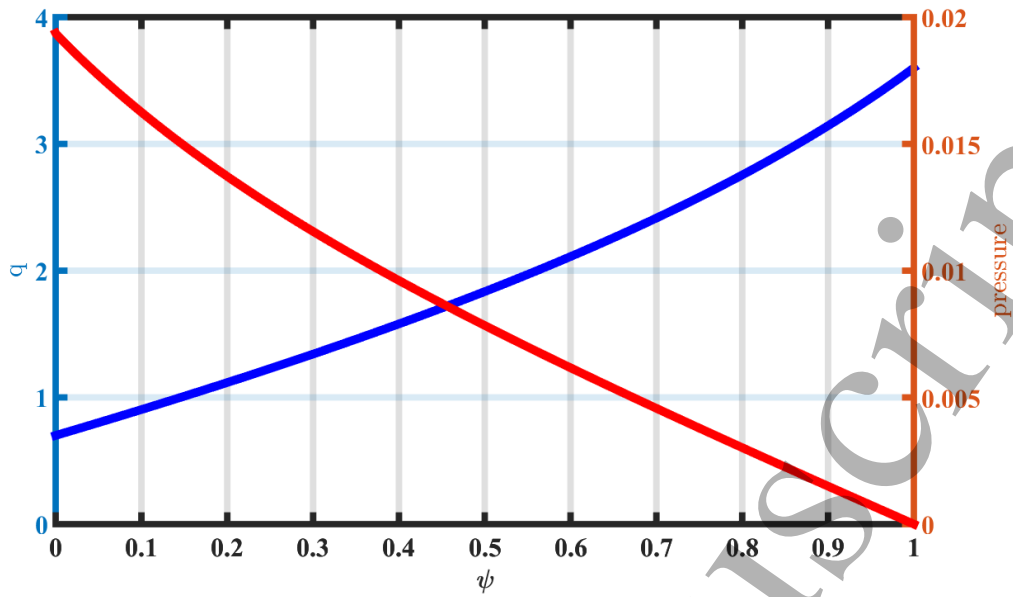
Figure 1   Initial safety factor q and pressure profiles.

Figure 2 Evolution of the kinetic energy with $\nu=1.0\times10^{-4}$. The period of the normal

sawtooth oscillation is $T\sim4970t_{\mathrm{A}}$.

The evolution of the kinetic energy with $\nu=1.0\times10^{-4}$ is shown in Figure 2. As

we can see, the oscillation exhibits the normal sawtooth behavior with period

$T\sim4970t_{\mathrm{A}}$. The evolution of the plasma pressure profile along Z=0 and $\varphi=0$ is

shown in Figure 3. The pressure profile also exhibits periodic oscillations with the period $T \sim 4970t_A$. Since the normal sawtooth has been intensively investigated in past decades [40, 49], we will not discuss the normal sawtooth in more details in the present paper.

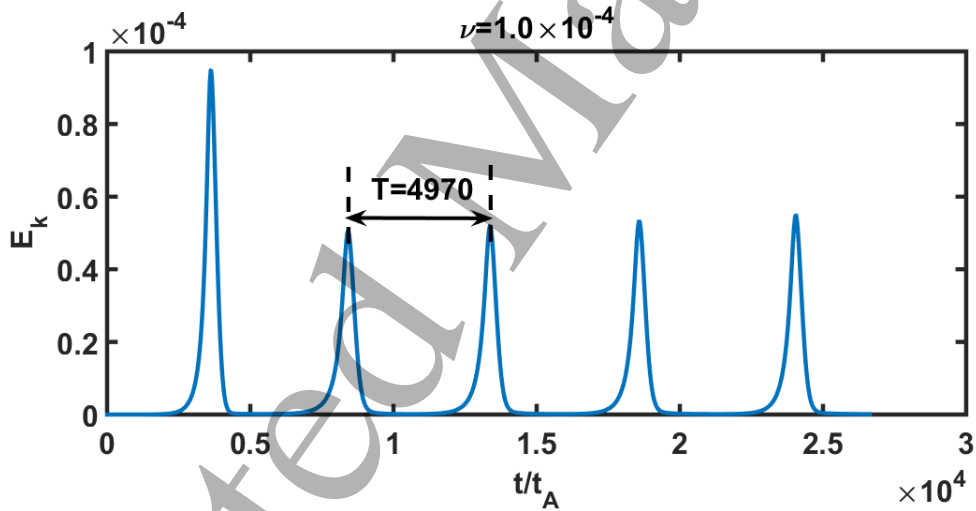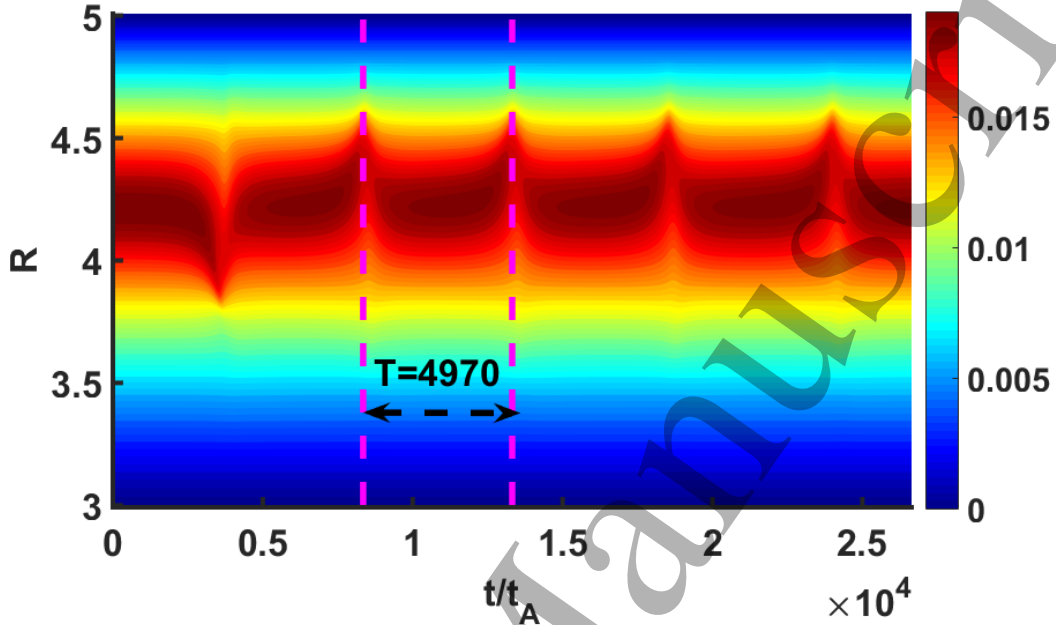Figure 3 Evolution of the plasma pressure profile along Z=0 with $\nu=1.0\times10^{-4}$. The pressure profile exhibits periodic oscillations with the period $T \sim 4970t_A$.

More interestingly, when viscosity is reduced to $\nu=2.0\times10^{-5}$, the amplitude of the sawtooth oscillation becomes smaller and we enter what we refer to as the small sawtooth scenario. The evolution of the kinetic energy and of the pressure profile for this case is shown in Figures 4 and 5, respectively, where it can be seen that the period of the small sawtooth oscillations is reduced to $T \sim 1300t_A$. The value of the peak pressure is lower in this case as compared with that of a normal sawtooth, which suggests that, after the first massive pressure crash, the system never fully recovers during the small sawtooth (Figure 5), while it is almost fully recovered during the normal sawtooth (Figure 3). Such kind of behavior could also be seen from the Poincare plots of magnetic field lines (Figure 6a and b).

Also, for this small sawtooth scenario, the m/n=1 magnetic island never evolves so as to occupy the entire region with q initially below unity, while it does so for the normal sawtooth. In other words, Kadomtsev's full reconnection is not observed in our simulations in the small sawtooth regime, while it is confirmed by our simulations at larger viscosity exhibiting normal sawtooth behavior. For the small sawtooth scenario, the magnetic island pulsates between a smaller and a larger amplitude.

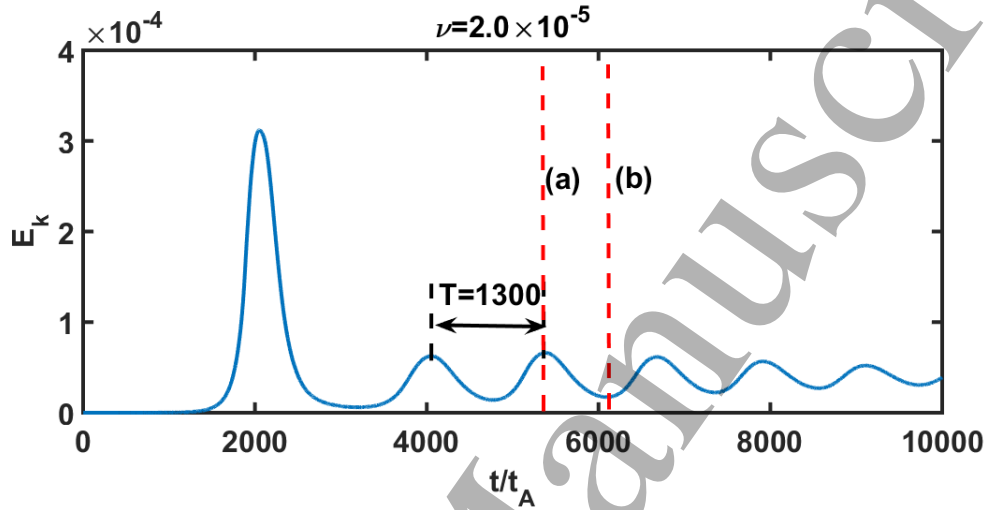

Figure 4 Evolution of the kinetic energy with ν=2.0×10^{-5}. The sawtooth shows small oscillations with a shorter period $T\sim1300t_A$. The peak time (a) $t = 5328t_A$ and the end time (b) $t = 6127t_A$ of the third cycle are labeled with vertical red dash lines.
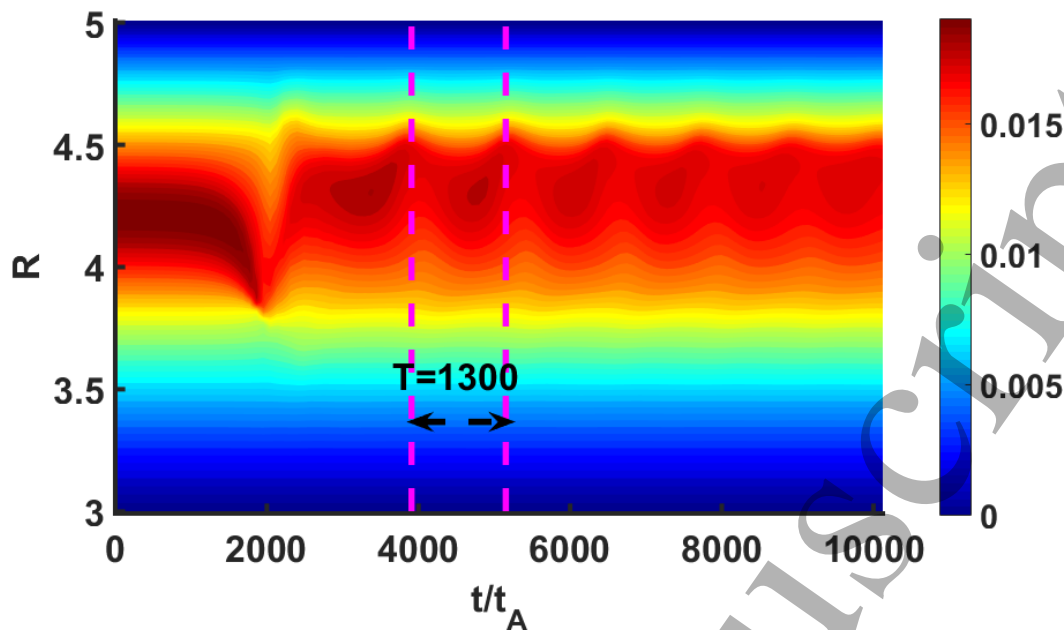
Figure 5 Evolution of the pressure profile at Z=0 with $\nu=2.0\times10^{-5}$. It is clear that, after the first crash, the pressure of the hot core is much lower for the small sawtooth than for the normal sawtooth, which suggests that the system is not able to fully recover during the small sawtooth.
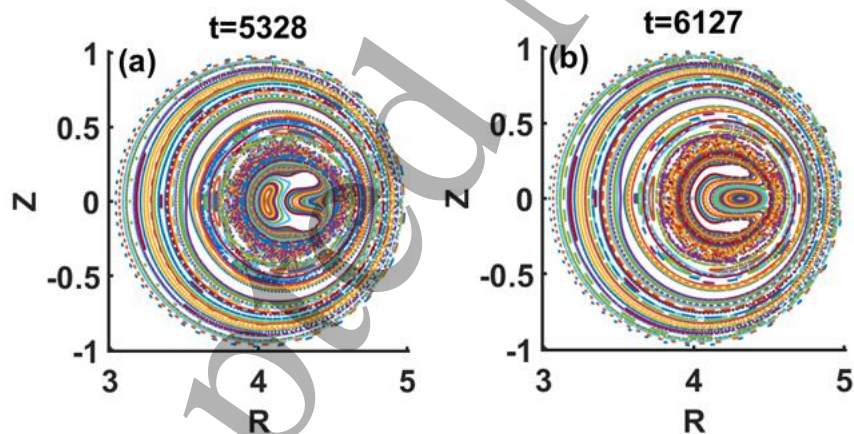
Figure 6 Poincare plots of magnetic field lines at (a) $t=5328t_A$ and (b) $t=6127t_A$ for the small sawtooth. The m/n=1 magnetic island is not fully developed as it does in the normal sawtooth oscillation.

As the viscosity is further reduced to $\nu=6.0\times10^{-6}$, the system evolves into a

steady-state. As shown in Figure 7 and Figure 8, the kinetic energy and the pressure profile remain almost unchanged after $t = 6000t_A$, which means that the system does evolve spontaneously towards a steady-state. The Poincare plots of magnetic field lines in the steady-state are shown in Figure 9. Eventually, the system reaches the steady-state with a non-axisymmetric, helical magnetic field structure, which is similar to the hybrid scenario often observed in many Tokamak experiments [26, 50-54]
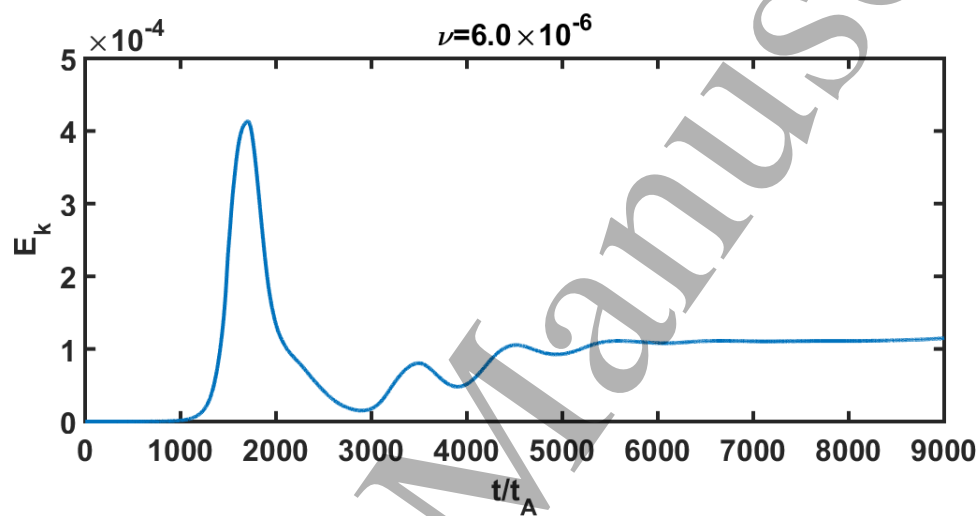
Figure 7   Evolution of the kinetic energy with $\nu=6.0\times10^{-6}$. After the first massive crash, the system evolves into a stationary state, and the kinetic energy almost remains unchanged after $t = 6000t_A$.

Figure 8 Evolution of the pressure profile at Z=0 with $\nu=6.0\times10^{-6}$. After $t=6000t_A$, the pressure profile almost remains unchanged.

Figure 9   Poincare plot in the steady-state of sawtooth oscillations at low viscosity ($\nu=6.0\times10^{-6}$).

In order to investigate the steady-state scenario found in Ref. [28], we have

increased viscosity to the unrealistic high value $\nu=1.0\times10^{-3}$. Indeed, it is found that also in this case sawtooth oscillations could also gradually evolve into a steady-state, as shown in Figure 10 and Figure 11. The kinetic energy and the pressure profiles remain almost unchanged after $t=25000t_A$. The Poincare plot of magnetic field lines at the steady-state stage is shown in Figure 12.

Therefore, from the simulation results presented in this subsection, we conclude that the system can eventually evolve toward a steady-state either at very high or at relatively low viscosity values. The normal sawtooth oscillation is observed to occur in the intermediate viscosity regime.
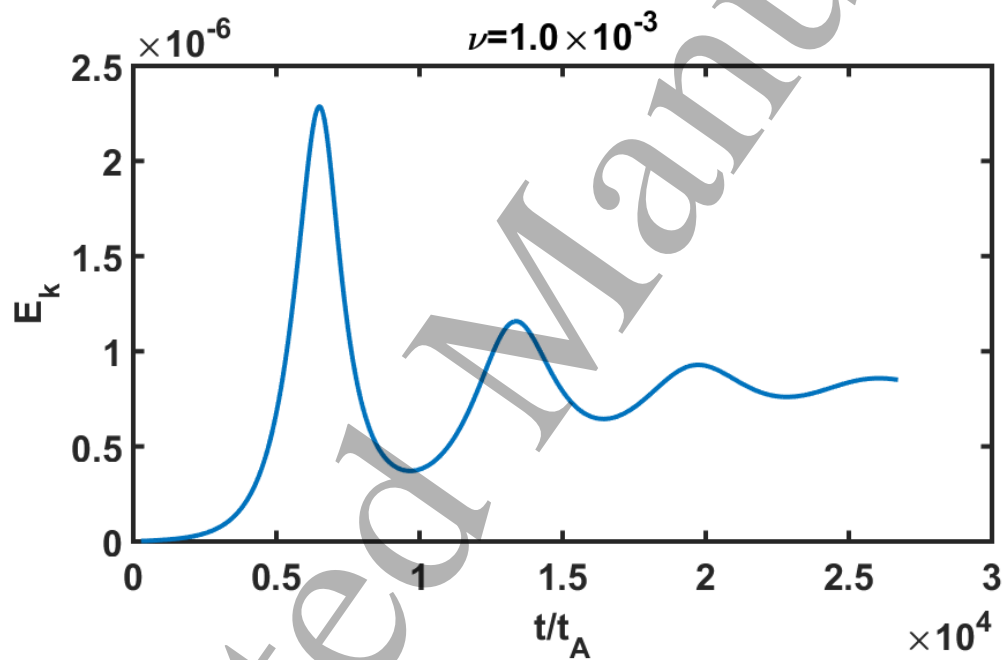
Figure 10 Evolution of the kinetic energy with $\nu=1.0\times10^{-3}$. After several cycles, the system eventually evolves into a stationary state, and the kinetic energy almost remains unchanged after $t=25000t_A$.
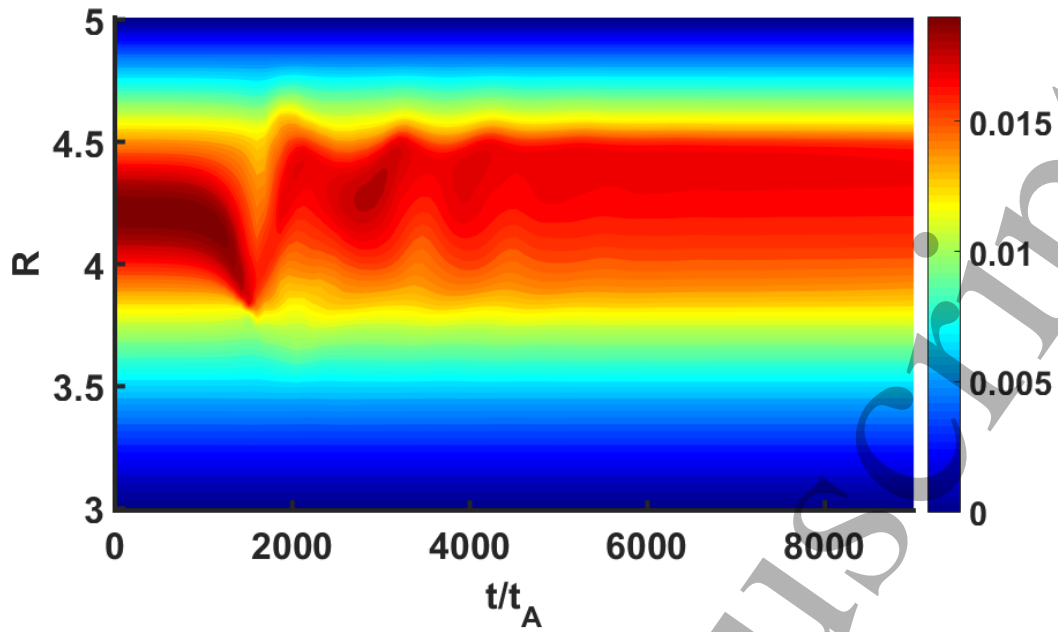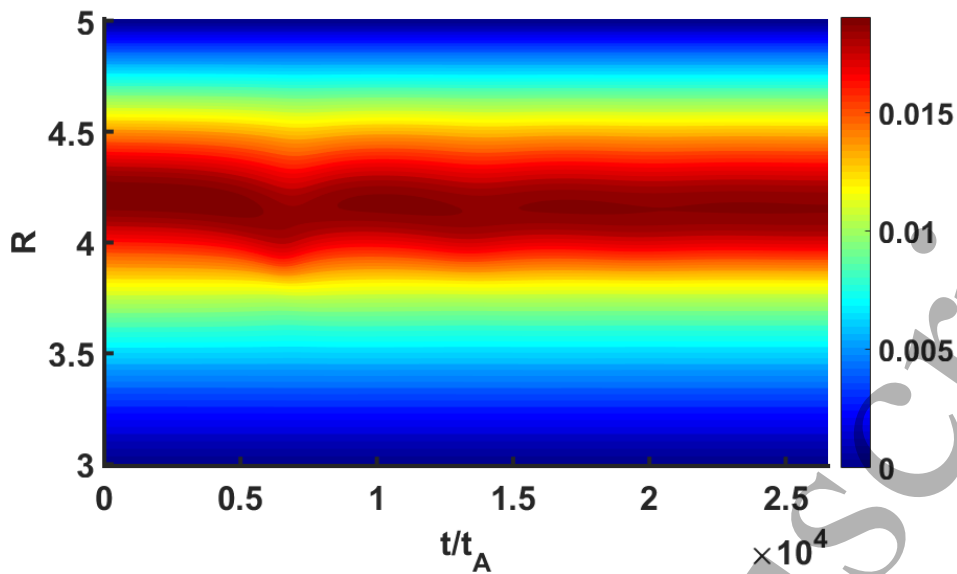
Figure 11 Evolution of the pressure profile at Z=0 with $\nu=1.0\times10^{-3}$. After $t = 25000t_A$, the pressure profile almost remains unchanged.
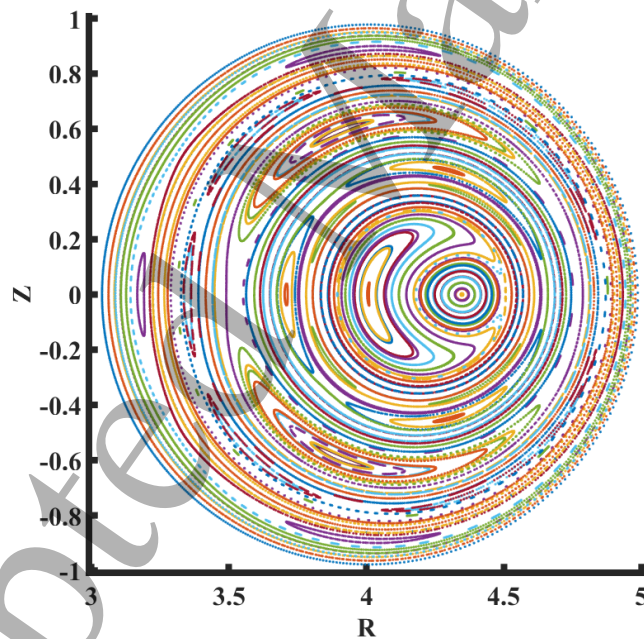
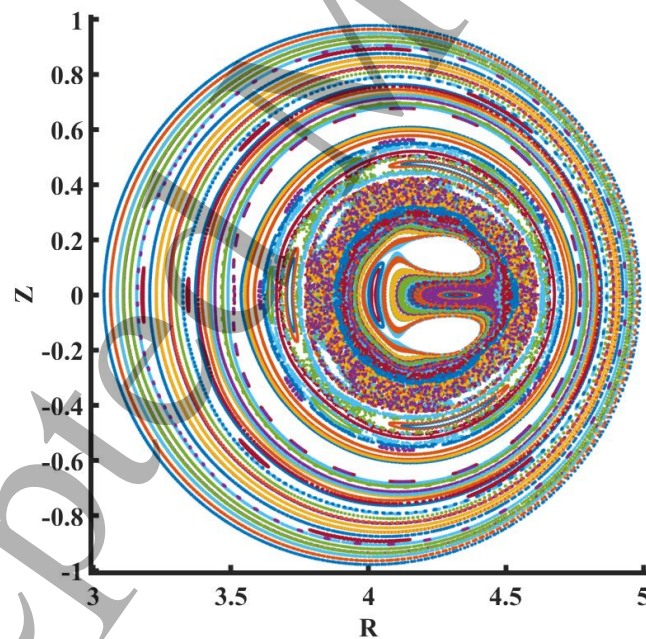Figure 12 Poincare plots in the steady-state of sawtooth oscillations with the high viscosity ($\nu=1.0\times10^{-3}$).

B. Sawtooth oscillations with low β

It should be noted that Shen and Porcelli [28] only presented the sawtooth

behavior in the regime of relatively high viscosity, $\nu \geq 1.0 \times 10^{-3}$, and relatively low plasma beta, $\beta = 0.2\%$. Their results indicate that the system exhibits a normal sawtooth oscillation at lower viscosity, while the sawtooth magnetic island eventually evolves toward a steady-state at higher viscosity. Therefore, we carry out simulations with a broader range of viscosity values and the same plasma beta, $\beta = 0.2\%$, to check whether the system could turn into a steady-state at sufficient low viscosity. Other parameters and the initial profiles are the same as in Section III. A. The evolution of the kinetic energy with $\nu = 1.0 \times 10^{-3}$, $\nu = 1.0 \times 10^{-4}$, $\nu = 1.0 \times 10^{-5}$, and $\nu = 1.0 \times 10^{-6}$ is shown in Figure 13. With $\nu = 1.0 \times 10^{-3}$, the system evolves into a steady-state after several oscillations. In contrast, sawtoothing behavious is always observed at lower viscosity values, namely, $\nu = 1.0 \times 10^{-4}$ or $\nu = 1.0 \times 10^{-5}$. These plots of kinetic energy as function of time shown here in Fig. 13 are similar to the plots of Figure 10 in Ref. [28]. However, we also find that with sufficient low viscosity, namely $\nu = 1.0 \times 10^{-6}$, the system can also turn into a steady-state. As we remarked earlier, this low viscosity regime was not studied in Ref. [28].
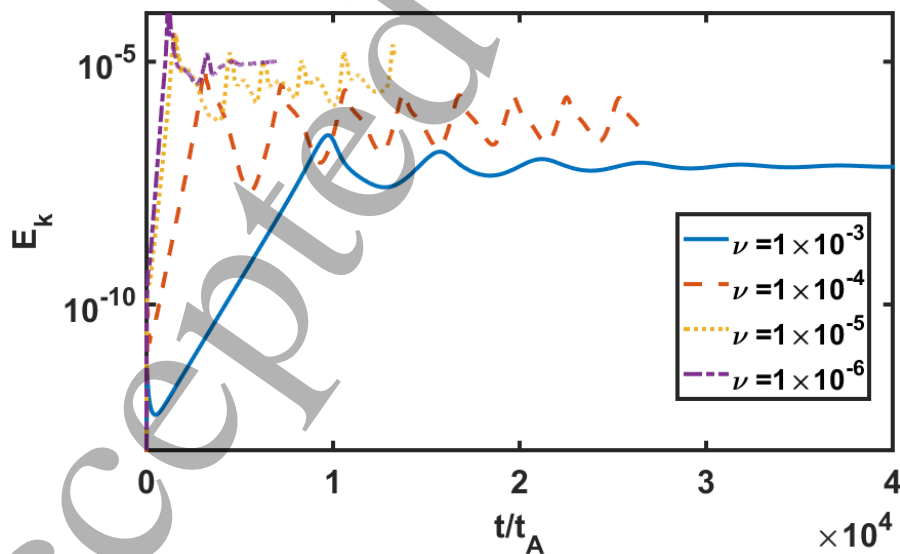
Figure 13 Evolutions of the kinetic energy with $\nu = 1.0 \times 10^{-3}$, $\nu = 1.0 \times 10^{-4}$, $\nu = 1.0 \times 10^{-5}$, and $\nu = 1.0 \times 10^{-6}$.

C. β scanning

From Subsection III. A and B, the middle parameter regime for the normal sawtooth is broadened when the plasma beta is lower. Therefore, we systematically investigate the influence of β on sawtooth dynamics. The long-time behavior of the sawtooth oscillations at different β and viscosity values is shown in Figure 14. The normal sawtooth oscillations are labeled with blue diamonds. Since the small sawtooth oscillations reach a steady-state after several cycles, we label both small sawtooth oscillations and steady-states with red squares. As shown in Figure 14, the normal sawtooth only occurs in the intermediate viscosity regime, while the small sawtooth or the steady-state happens in the high or low viscosity regimes ($\nu \geq 1.0\times10^{-3}$ or $\nu \leq 1.0\times10^{-5}$). It is clear that the steady-state discussed in Ref. [28] is just the steady-state in the high viscosity regime.
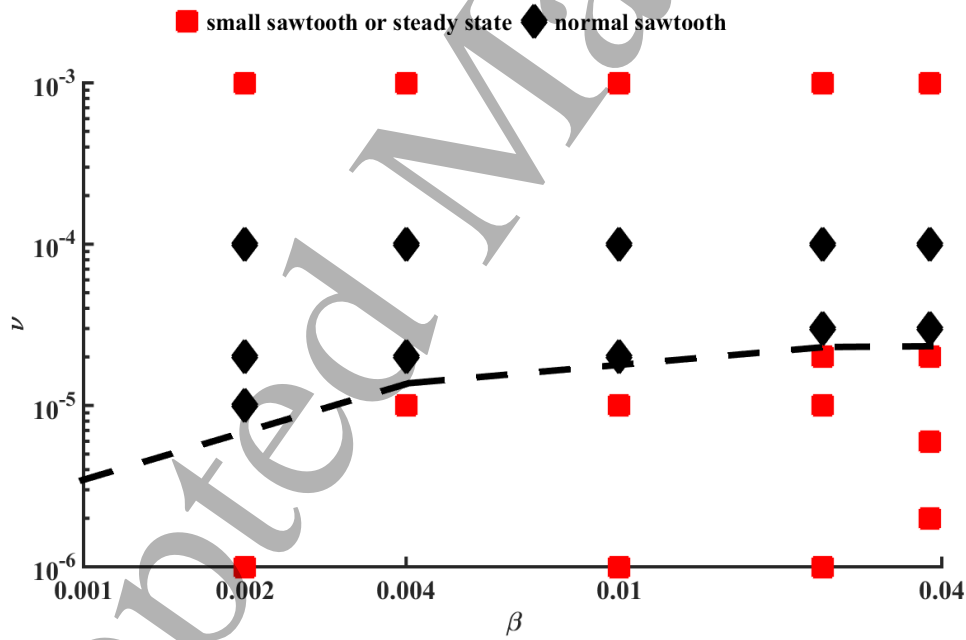
Figure 14 Long-time behaviors of sawtooth oscillations with different β and viscosities.
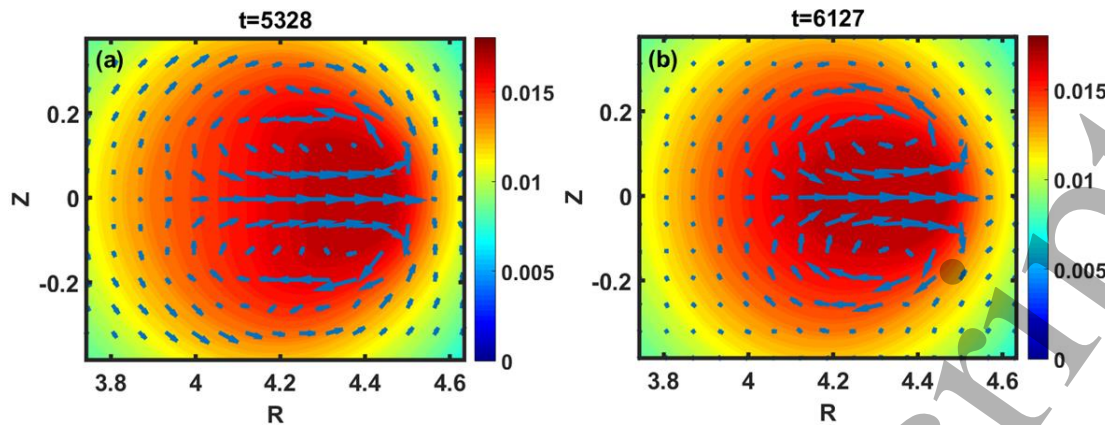
Figure 15 Flow patterns (the arrows) and pressure distributions (the contour plot) at (a) $t = 5328t_A$ just before the crash and (b) $t = 6127t_A$ after the crash for a small sawtooth. The flow is not entirely damped out at the end of the small sawtooth cycle. All the vectors are normalized by the maximum velocity in (a).

D.   Physical mechanism for the steady-state in the low viscosity regime

As shown in the previous subsections, we know that the system can evolve into (a) a steady-state with an extremely high viscosity, (b) a normal sawtooth with a medium viscosity, (c) a small sawtooth oscillation with a lower viscosity, and (d) a steady-state with a sufficient low viscosity. The steady-state with an extremely high viscosity is easy to understand, As shown by Shen and Porcelli,[28] helical plasma flows in the high viscosity regime are considerably damped within the time scale of a sawtooth ramp, to the point that the near absence of these flows prevents further growth of the m/n=1 magnetic island, leading to a high-viscosity saturated island state. Then, the question is, what mechanism leads to the system evolving into a steady-state with a sufficiently low viscosity?
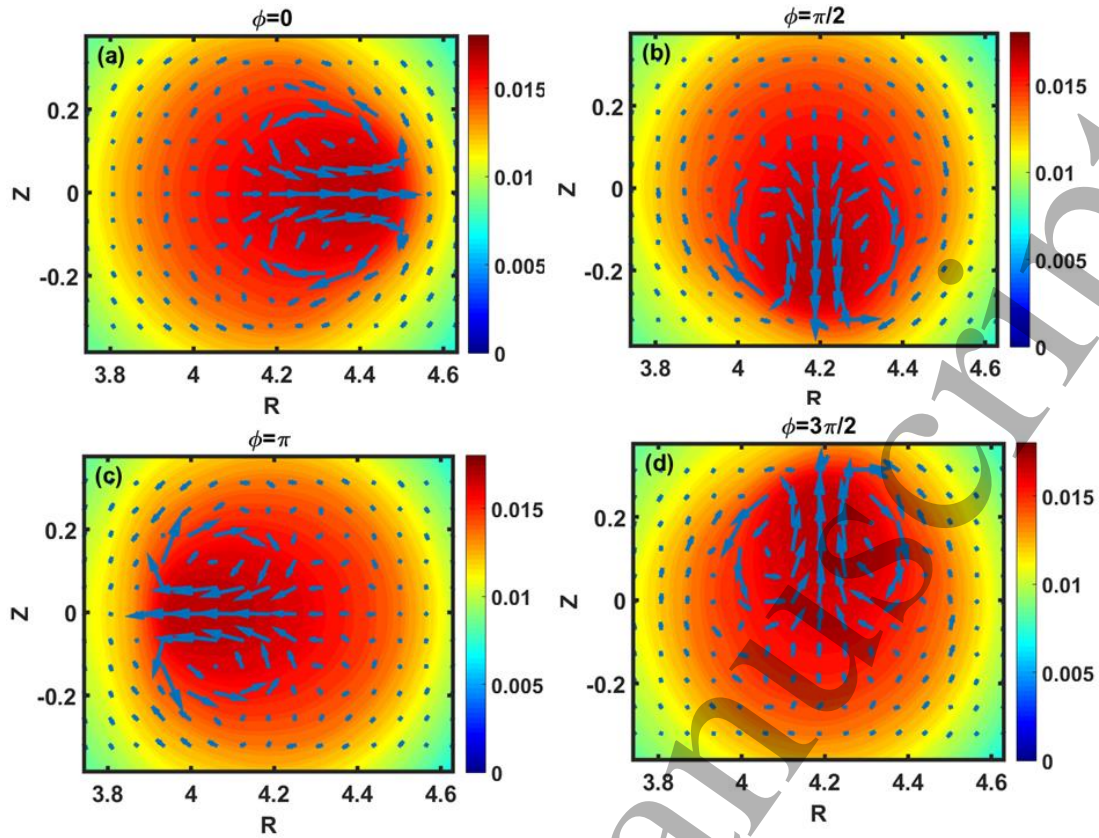
Figure 16 Flow patterns of the stationary state at $\phi=0$, $\phi=\pi/2$, $\phi=\pi$ and $\phi=3\pi/2$, respectively. All the vectors are normalized by the maximum velocity during the simulations of the steady-state. It is evident that there exists a strong residual flow with the $m=n=1$ helicity at the steady-state.

From the evolutions of the kinetic energy, as shown in Figures 2, 4, and 7, the remarkable difference in these three cases is the residual flow after a sawtooth cycle. For the case with normal sawtooth oscillations, there is no residual flow since the kinetic energy is almost zero after each sawtooth crash, as shown in Figure 2. However, for the cases with small sawtooth oscillations and for the steady-state scenario, the kinetic energy does not decrease to zero. Instead, it increases on average after the first sawtooth cycle, as shown in Figures 4 and 7. The finite kinetic energy means that there is a notable residual flow, which is quite evident in Figures 15 and 16. It should be noted that the magnetic flux is approximately frozen in the plasma except for the reconnection region. Since the direction of the residual flow is from the core to the reconnection region, it continuously carries magnetic flux into the reconnection region due to the frozen-in condition. It should also be noted that, in our model, the

newly pumped magnetic flux is mainly due to the magnetic pump term in the Ohm's law (Eq. 5), as discussed earlier. Since the toroidal current is significantly reduced from the initial value, new magnetic flux is continuously pumped in the core region. Therefore, the steady-state results from the balance between the newly pumped poloidal magnetic flux in the core region and the poloidal magnetic flux that is destroyed by the reconnection process. The residual flow is regarded as the 'bridge' between the pumped poloidal magnetic flux and the dissipated magnetic flux. The current density profiles for the initial equilibrium and the steady-states in the limits of low and high viscosities are shown in Figure 17, which suggests that the mechanism for the steady-state with a very low viscosity results from the combination of the magnetic pump effect in the core region, the fast reconnection due to a thin and sharp current sheet at the resonant surface, and the large residual flow (Figure 16).
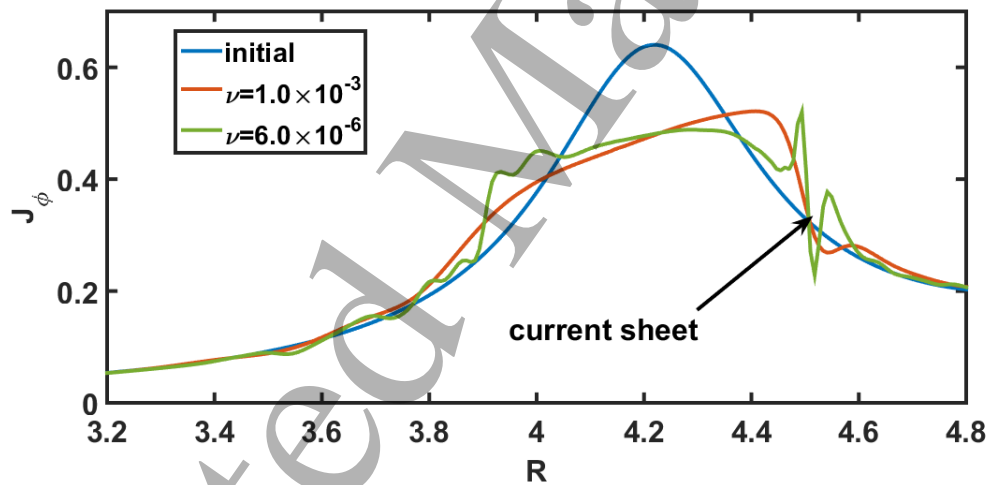
Figure 17 The current density profiles for the initial equilibrium and the steady-states in the cases with the low and high viscosities.

It should also be noted that the intermediate viscosity regime for the normal sawtooth becomes broader with decreasing plasma beta (Figure 14). The lower boundary of the intermediate regime increases from $\nu=1.0\times10^{-6}$ for the low β cases to $\nu=2.0\times10^{-5}$ for the high β cases. Figure 18 clearly shows that the residual flow decreases with decreasing β. Therefore, lower viscosity is required in order to

generate enough residual flow necessary for achieving steady-state. Since the final residual flow increases with increasing β, the saturated amplitude of the saturated m/n=1 magnetic island also increases with increasing β, and so does the radial displacement of the magnetic axis in the saturated state.
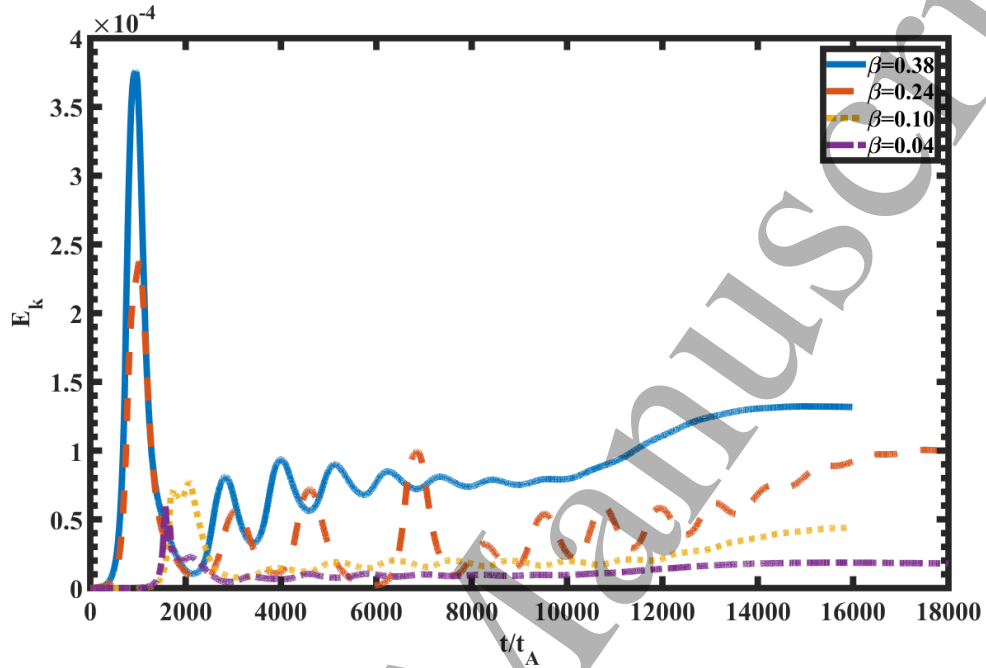
Figure 18 Evolutions of the kinetic energy with ν=1.0$\times$10^{-5} and different β.
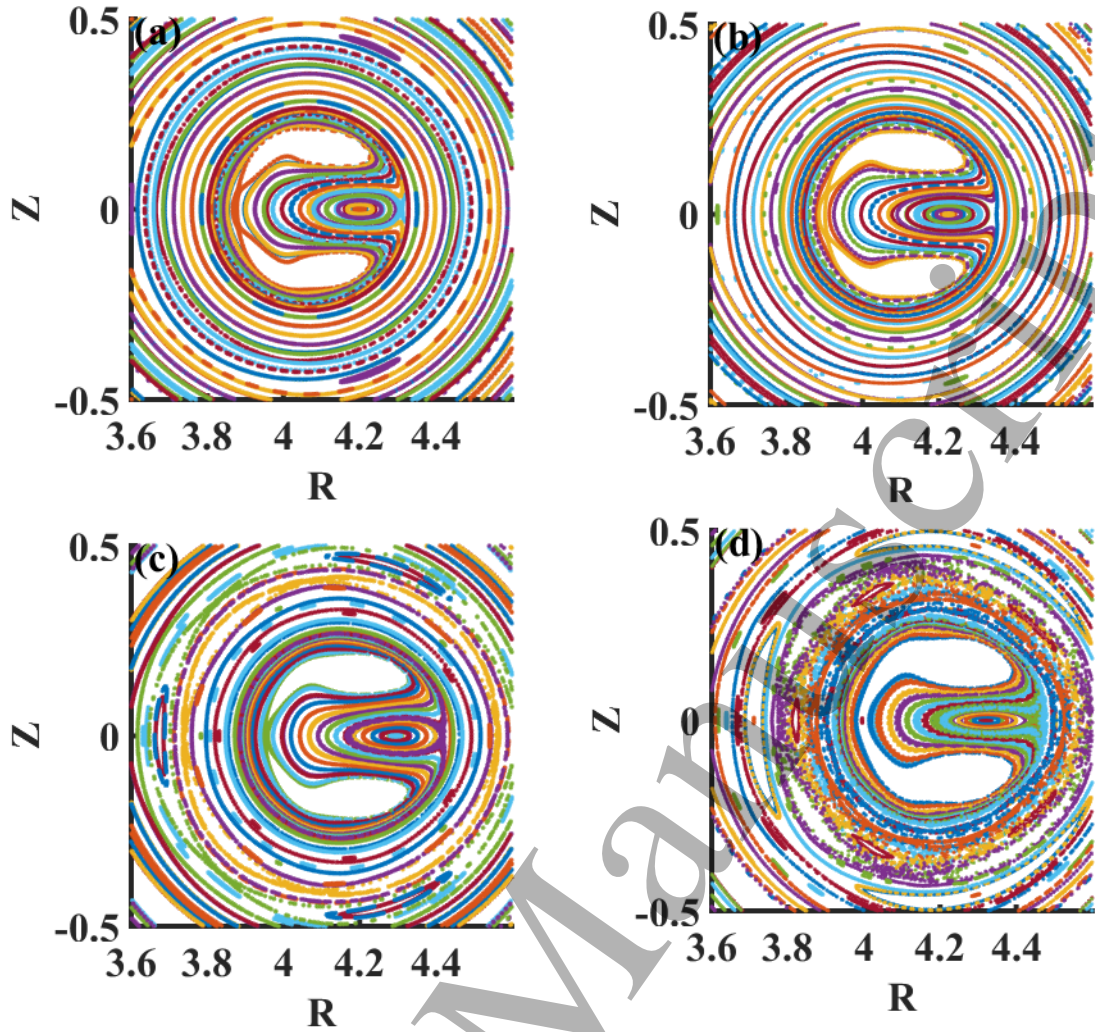
Figure 19   The Poincare plots of the magnetic field at the stationary state with different initial plasma (a) β=0.04, (b) β=0.10,(c) β=0.24, and (d) β=0.38. At the stationary state, the radial displacement of the magnetic axis and the widths of the m/n=1 magnetic island increases with increasing β.

E.   Influence of electron diamagnetic drifts.

The influence of the electron diamagnetic drift on the two types of steady-state is investigated in this subsection by turning on the Hall term (two-fluid effect). The kinetic energy evolutions with $\nu = 1 \times 10^{-3}$ $d_i = 0$ (blue solid line), $\nu = 1 \times 10^{-3}$ $d_i = 0.03$ (blue dashed line), $\nu = 1 \times 10^{-6}$ $d_i = 0$ (red solid line), and $\nu = 1 \times 10^{-6}$ $d_i = 0.03$ (red dashed line) are shown in Figure 20. Although the electron diamagnetic drift can slightly modify the energy evolution, the nature of the steady-state magnetic island at both high and low viscosity values is not strongly affected. In other words, in the limits of high or low viscosity, the system is still observed to evolve into a steady-state even in the presence of two-fluids effects. With

$d_i = 0.03$, the electron diamagnetic frequency $\omega_{*e} = 0.0012$, and the ion-sound

Larmor radius $\rho_s = p^{\frac{1}{2}} d_i = 0.0037$ on the $q = 1$ resonant surface (where

$p = 0.0149$ is the normalized plasma pressure). The linear growth rate of the

resistive-kink mode is about $\gamma_L = 0.009$ for the low viscosity case, and the linear

width of the restive internal kink is $\delta = 0.0054$. Note that ρ_s is smaller than δ and

γ_L is larger than ω_{*e}. It is why the two-fluids effects play a negligible role in our

simulations.
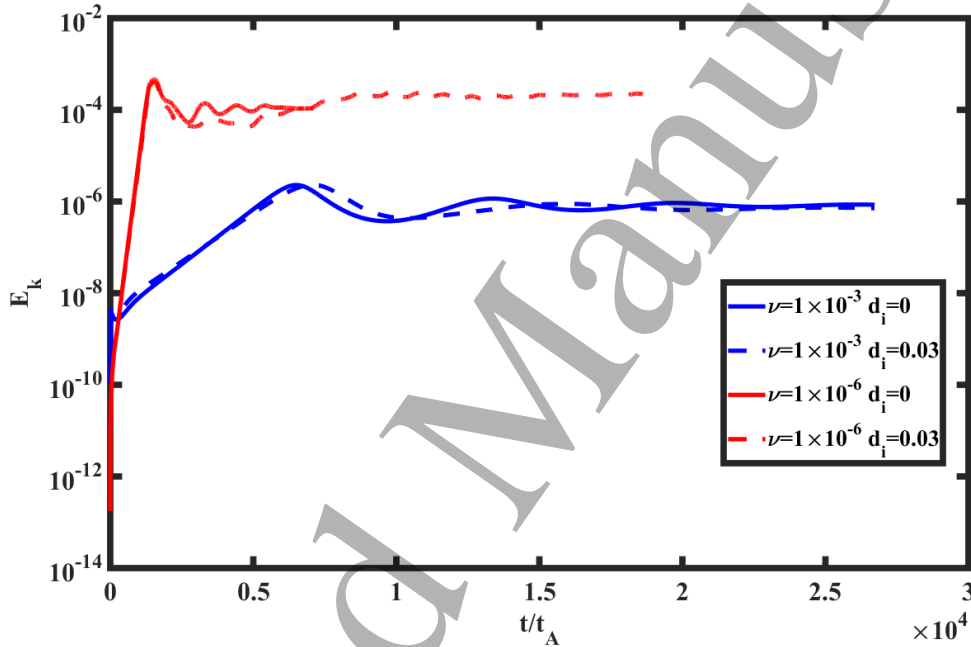
Figure 20 The kinetic energy evolution with $\nu = 1 \times 10^{-3}$ $d_i = 0$ (blue solid line),

$\nu = 1 \times 10^{-3}$ $d_i = 0.03$ (blue dashed line), $\nu = 1 \times 10^{-6}$ $d_i = 0$ (red solid line), and

$\nu = 1 \times 10^{-6}$ $d_i = 0.03$ (red dashed line).

IV. Conclusions

In this article, we have carried out numerical simulations aimed at a systematic

study on the influence of plasma viscosity and of the plasma β (=kinetic

pressure/magnetic pressure) parameter on the nonlinear evolution of resistive internal

kink modes, which are considered to be responsible for sawtooth relaxation oscillations in tokamak plasmas. In Ref.[28], it was found that the plasma can evolve nonlinearly towards a steady state with a saturated m/n=1 magnetic island in the limit of very large viscosity. However, the values of the relevant magnetic Prandtl number (viscosity/resistivity) needed to achieve the steady state regime of Ref. [28] are unrealistically high when considering the parameters of present day tokamak experiments. By contrast, the main result of our work is that a new regime with relatively low viscosity exists, such that sawtooth oscillations are also found to spontaneously evolve towards states with stationary m/n=1 magnetic islands. Thus, numerical simulations indicate that the plasma can evolve into the so-called small sawtooth oscillation regime and eventually into a steady state with a saturated magnetic island in the two opposite limits of high and low viscosity. For intermediate viscosity values, the more standard, normal sawtooth regime is found.

It is suggested that the mechanism at work in the limit of small viscosity is related to magnetic flux pumping, a concept first discussed in Refs.[42, 43] However, while in recent studies[27, 44] flux pumping maintains the q profile close to and above unity, thus preventing the onset of m/n=1 magnetic islands, in our case flux pumping allied with the nonlinear resistive internal kink dynamics leads to a stationary helical flow, only weakly dissipated by viscosity, which is entirely self-consistent with the presence of a saturated m/n=1 stationary magnetic island.

Thus, flux pumping in our simulations is associated with the possibility of a sufficiently large, nonlinear helical plasma flow. If viscosity is relatively high, the nonlinear flow is largely dissipated [28]. However, in the low viscosity regime, the residual flow after each sawtooth crash remains sufficiently large. Due to the frozen-in condition, the residual flow continuously carries magnetic flux from the plasma core to the reconnection region near the island X-point. This could be described as a kind of magnetic pump mechanism. Thus, the observed steady-state regime with a saturated m/n=1 magnetic island can be understood as the result of a balance between magnetic flux generated by the magnetic pump in the core region and magnetic flux dissipated in the reconnection region.

It is also found that the threshold viscosity value for the onset of the steady state regime depends on β. More specifically, the low-viscosity steady state regime can occur for values of the viscosity parameter below a critical threshold, whose value increases with increasing β. This can be easily understood: the drive for the resistive internal kink mode is stronger at higher beta, which results in a stronger nonlinear helical flow. The persistence on the nonlinear helical flow is necessary for the flux pumping mechanism to be effective. Since viscosity tends to damp the nonlinear flow, the low-viscosity steady state regime can extend to higher values of the viscosity parameter at higher β values.

In conclusion, the newly found regime for steady-state m/n=1 magnetic islands may be relevant for the understanding of tokamak experiments, where indeed saturated helical structures such as the density snake [36-38] and steady-state magnetic islands are sometimes observed in the core plasma region where the safety factor is close to or below unity [26, 50-55].

The limitation of the present analysis, similarly to the case of most numerical simulations of tokamak plasmas published in the literature, is that values of resistivity and viscosity in the range of 10^{-6} or higher are used in this article. It remains to be established where the results of this work can be extrapolated to the even lower values of resistivity and viscosity realized in present-day tokamak plasmas. Nevertheless, in terms of the relevant magnetic Prandtl number defined as the ratio between viscosity and resistivity, the low viscosity steady state regime found in this article requires values of the magnetic Prandtl number that are realistic for present-day tokamak experiments.

Acknowledgment

References

[1] S. von Goeler, W. Stodiek, N. Sauthoff, Studies of Internal Disruptions and m=1 Oscillations in Tokamak Discharges with Soft X-Ray Tecniques, Physical Review Letters, 33 (1974) 1201-1203.

[2] K. McGuire, D.C. Robinson, Sawtooth oscillations in a small tokamak, Nuclear Fusion, 19 (1979) 505.

[3] M.A. Dubois, A.L. Pecquet, C. Reverdin, Internal disruptions in the TFR tokamak: A phenomenological analysis, Nuclear Fusion, 23 (1983) 147.

[4] T.C. Hender, J.C. Wesley, J. Bialek, A. Bondeson, A.H. Boozer, R.J. Buttery, A. Garofalo, T.P. Goodman, R.S. Granetz, Y. Gribov, O. Gruber, M. Gryaznevich, G. Giruzzi, S. Günter, N. Hayashi, P. Helander, C.C. Hegna, D.F. Howell, D.A. Humphreys, G.T.A. Huysmans, A.W. Hyatt, A. Isayama, S.C. Jardin, Y. Kawano, A. Kellman, C. Kessel, H.R. Koslowski, R.J.L. Haye, E. Lazzaro, Y.Q. Liu, V. Lukash, J. Manickam, S. Medvedev, V. Mertens, S.V. Mirnov, Y. Nakamura, G. Navratil, M. Okabayashi, T. Ozeki, R. Paccagnella, G. Pautasso, F. Porcelli, V.D. Pustovitov, V. Riccardo, M. Sato, O. Sauter, M.J. Schaffer, M. Shimada, P. Sonato, E.J. Strait, M. Sugihara, M. Takechi, A.D. Turnbull, E. Westerhof, D.G. Whyte, R. Yoshino, H. Zohm, D. the Itpa Mhd, G. Magnetic Control Topical, Chapter 3: MHD stability, operational limits and disruptions, Nuclear Fusion, 47 (2007) S128.

[5] A. Letsch, H. Zohm, F. Ryter, W. Suttrop, A. Gude, F. Porcelli, C. Angioni, I. Furno, Incomplete reconnection in sawtooth crashes in ASDEX Upgrade, Nuclear Fusion, 42 (2002) 1055.

[6] I. Furno, C. Angioni, F. Porcelli, H. Weisen, R. Behn, T.P. Goodman, M.A. Henderson, Z.A. Pietrzyk, A. Pochelon, H. Reimerdes, E. Rossi, Understanding sawtooth activity during intense electron cyclotron heating experiments on TCV, Nuclear Fusion, 41 (2001) 403.

[7] A.W. Edwards, D.J. Campbell, W.W. Engelhardt, H.U. Fahrbach, R.D. Gill, R.S. Granetz, S. Tsuji, B.J.D. Tubbing, A. Weller, J. Wesson, D. Zasche, Rapid Collapse of a Plasma Sawtooth Oscillation in the JET Tokamak, Physical Review Letters, 57 (1986) 210-213.

[8] K. McGuire, V. Arunasalam, C.W. Barnes, M.G. Bell, M. Bitter, R. Boivin, N.L. Bretz, R. Budny, C.E. Bush, A. Cavallo, T.K. Chu, S.A. Cohen, P. Colestock, S.L. Davis, D.L. Dimock, H.F. Dylla, P.C. Efthimion, A.B. Ehrhrardt, R.J. Fonck, E. Fredrickson, H.P. Furth, G. Gammel, R.J. Goldston, G. Greene, B. Grek, L.R. Grisham, G. Hammett, R.J. Hawryluk, H.W. Hendel, K.W. Hill, E. Hinnov, D.J. Hoffman, J. Hosea, R.B. Howell, H. Hsuan, R.A. Hulse, A.C. Janos, D. Jassby, F. Jobes, D.W. Johnson, L.C. Johnson, R. Kaita, C. Kieras‐Phillips, S.J. Kilpatrick, P.H. LaMarche, B. LeBlanc, D.M. Manos, D.K. Mansfield, E. Mazzucato, M.P. McCarthy, M.C. McCune, D.H. McNeill, D.M. Meade, S.S. Medley, D.R. Mikkelsen, D. Monticello, R. Motley, D. Mueller, J.A. Murphy, Y. Nagayama, D.R. Nazakian, E.B. Neischmidt, D.K. Owens, H. Park, W. Park, S. Pitcher, A.T. Ramsey, M.H. Redi, A.L. Roquemore, P.H. Rutherford, G. Schilling, J. Schivell, G.L. Schmidt, S.D. Scott, J.C. Sinnis, J. Stevens, B.C. Stratton, W. Stodiek, E.J. Synakowski, W.M. Tang, G. Taylor, J.R. Timberlake, H.H. Towner, M. Ulrickson, S.v. Goeler, R. Wieland, M. Williams, J.R. Wilson, K.L. Wong, M. Yamada, S. Yoshikawa, K.M. Young, M.C. Zarnstorff, S.J. Zweben, High‐beta operation and magnetohydrodynamic activity on the TFTR tokamak, Physics of Fluids B: Plasma Physics, 2 (1990) 1287-1290.

[9] D.J. Campbell, R.D. Gill, C.W. Gowers, J.A. Wesson, D.V. Bartlett, C.H. Best, S. Coda, A.E. Costley, A. Edwards, S.E. Kissel, R.M. Niestadt, H.W. Piekaar, R. Prentice, R.T. Ross, B.J.D. Tubbing, Sawtooth activity in ohmically heated JET plasmas, Nuclear Fusion, 26 (1986) 1085-1092.

[10] O. Sauter, E. Westerhof, M.L. Mayoral, B. Alper, P.A. Belo, R.J. Buttery, A. Gondhalekar, T. Hellsten,

T.C. Hender, D.F. Howell, T. Johnson, P. Lamalle, M.J. Mantsinen, F. Milani, M.F.F. Nave, F. Nguyen, A.L. Pecquet, S.D. Pinches, S. Podda, J. Rapp, Control of Neoclassical Tearing Modes by Sawtooth Control, Physical Review Letters, 88 (2002) 105001.

[11] R.J. Buttery, T.C. Hender, D.F. Howell, R.J.L. Haye, O. Sauter, D. Testa, Onset of neoclassical tearing modes on JET, Nuclear Fusion, 43 (2003) 69.

[12] D.J. Campbell, D.F.H. Start, J.A. Wesson, D.V. Bartlett, V.P. Bhatnagar, M. Bures, J.G. Cordey, G.A. Cottrell, P.A. Dupperex, A.W. Edwards, C.D. Challis, C. Gormezano, C.W. Gowers, R.S. Granetz, J.H. Hammen, T. Hellsten, J. Jacquinot, E. Lazzaro, P.J. Lomas, N.L. Cardozo, P. Mantica, J.A. Snipes, D. Stork, P.E. Stott, P.R. Thomas, E. Thompson, K. Thomsen, G. Tonetti, Stabilization of Sawteeth with Additional Heating in the JET Tokamak, Physical Review Letters, 60 (1988) 2148-2151.

[13] R.J. Buttery, T.C. Hender, D.F. Howell, R.J.L. Haye, S. Parris, O. Sauter, C.G. Windsor, J.-E. Contributors, On the form of NTM onset scalings, Nuclear Fusion, 44 (2004) 678.

[14] I.T. Chapman, Controlling sawtooth oscillations in tokamak plasmas, Plasma Physics and Controlled Fusion, 53 (2011) 013001.

[15] M. Shimada, D.J. Campbell, V. Mukhovatov, M. Fujiwara, N. Kirneva, K. Lackner, M. Nagami, V.D. Pustovitov, N. Uckan, J. Wesley, N. Asakura, A.E. Costley, A.J.H. Donné, E.J. Doyle, A. Fasoli, C. Gormezano, Y. Gribov, O. Gruber, T.C. Hender, W. Houlberg, S. Ide, Y. Kamada, A. Leonard, B. Lipschultz, A. Loarte, K. Miyamoto, V. Mukhovatov, T.H. Osborne, A. Polevoi, A.C.C. Sips, Chapter 1: Overview and summary, Nuclear Fusion, 47 (2007) S1.

[16] G.H. Choe, G.S. Yun, H.K. Park, J.H. Jeong, Slow crash in modified sawtooth patterns driven by localized electron cyclotron heating and current drive in KSTAR, Nuclear Fusion, 58 (2018) 106038.

[17] M. Sertoli, T. Odstrcil, C. Angioni, A.U.T. the, Interplay between central ECRH and saturated (m , n) = (1, 1) MHD activity in mitigating tungsten accumulation at ASDEX Upgrade, Nuclear Fusion, 55 (2015) 113029.

[18] Z.Y. Cui, K. Zhang, S. Morita, X.Q. Ji, X.T. Ding, Y. Xu, P. Sun, J.M. Gao, C.F. Dong, D.L. Zheng, Y.G. Li, M. Jiang, D. Li, W.L. Zhong, L. Yi, Y.B. Dong, S.D. Song, L.M. Yu, Z.B. Shi, B.Z. Fu, P. Lu, M. Huang, B.S. Yuan, Q.W. Yang, X.R. Duan, Study of impurity transport in HL-2A ECRH L-mode plasmas with radially different ECRH power depositions, Nuclear Fusion, 58 (2018) 056012.

[19] E. Li, V. Igochine, O. Dumbrajs, L. Xu, K. Chen, T. Shi, L. Hu, The non-resonant kink modes triggering strong sawtooth-like crashes in the EAST tokamak, Plasma Physics and Controlled Fusion, 56 (2014) 125016.

[20] H.K. Park, N.C. Luhmann, A.J.H. Donné, I.G.J. Classen, C.W. Domier, E. Mazzucato, T. Munsat, M.J. van de Pol, Z. Xia, Observation of High-Field-Side Crash and Heat Transfer during Sawtooth Oscillation in Magnetically Confined Plasmas, Physical Review Letters, 96 (2006) 195003.

[21] Y. Sun, B. Wan, L. Hu, B. Shen, Understanding the m = 1 mode during the sawtooth ramp phase in lower hybrid current driven plasmas on the HT-7 tokamak, Nuclear Fusion, 47 (2007) 271.

[22] J.P. Graves, I.T. Chapman, S. Coda, M. Lennholm, M. Albergante, M. Jucker, Control of magnetohydrodynamic stability by phase space engineering of energetic ions in tokamak plasmas, Nature Communications, 3 (2012) 624.

[23] E. Lerche, M. Lennholm, I.S. Carvalho, P. Dumortier, F. Durodie, D.V. Eester, J. Graves, P. Jacquet, A. Murari, J.E.T. Contributors, Sawtooth pacing with on-axis ICRH modulation in JET-ILW, Nuclear Fusion, 57 (2017) 036027.

[24] D. Kim, T.P. Goodman, O. Sauter, Real-time sawtooth control and neoclassical tearing mode preemption in ITER, Physics of Plasmas, 21 (2014) 061503.

[25] Z. Chen, M. Nocente, M. Tardocchi, T. Fan, G. Gorini, Simulation of neutron emission spectra from neutral beam-heated plasmas in the EAST tokamak, Nuclear Fusion, 53 (2013) 063023.

[26] C.C. Petty, M.E. Austin, C.T. Holcomb, R.J. Jayakumar, R.J. La Haye, T.C. Luce, M.A. Makowski, P.A. Politzer, M.R. Wade, Magnetic-Flux Pumping in High-Performance, Stationary Plasmas with Tearing Modes, Physical Review Letters, 102 (2009) 045005.

[27] S.C. Jardin, N. Ferraro, I. Krebs, Self-Organized Stationary States of Tokamaks, Physical Review Letters, 115 (2015) 215001.

[28] W. Shen, F. Porcelli, Linear and nonlinear simulations of the visco-resistive internal kink mode using the M3D code, Nuclear Fusion, 58 (2018) 106035.

[29] B. Kadomtsev, Disruptive instability in Tokamaks(helical plasma motions), Soviet Journal of Plasma Physics, 1 (1975) 389-391.

[30] F. Porcelli, D. Boucher, M.N. Rosenbluth, Model for the sawtooth period and amplitude, Plasma Physics and Controlled Fusion, 38 (1996) 2163.

[31] F.D. Halpern, H. Lütjens, J.-F. Luciani, Diamagnetic thresholds for sawtooth cycling in tokamak plasmas, Physics of Plasmas, 18 (2011) 102501.

[32] F.D. Halpern, D. Leblond, H. Lütjens, J.F. Luciani, Oscillation regimes of the internal kink mode in tokamak plasmas, Plasma Physics and Controlled Fusion, 53 (2010) 015011.

[33] W. Zhang, Z.W. Ma, H.W. Zhang, J. Zhu, Dynamic evolution of resistive kink mode with electron diamagnetic drift in tokamaks, Physics of Plasmas, 26 (2019) 042514.

[34] X. Wang, A. Bhattacharjee, Nonlinear dynamics of the m=1 instability and fast sawtooth collapse in high-temperature plasmas, Physical Review Letters, 70 (1993) 1627-1630.

[35] A.Y. Aydemir, Nonlinear studies of m=1 modes in high‐temperature plasmas, Physics of Fluids B: Plasma Physics, 4 (1992) 3469-3472.

[36] L. Delgado-Aparicio, L. Sugiyama, R. Granetz, D.A. Gates, J.E. Rice, M.L. Reinke, M. Bitter, E. Fredrickson, C. Gao, M. Greenwald, K. Hill, A. Hubbard, J.W. Hughes, E. Marmar, N. Pablant, Y. Podpaly, S. Scott, R. Wilson, S. Wolfe, S. Wukitch, Formation and Stability of Impurity ``Snakes'' in Tokamak Plasmas, Physical Review Letters, 110 (2013) 065006.

[37] L. Delgado-Aparicio, L. Sugiyama, R. Granetz, D. Gates, J. Rice, M.L. Reinke, W. Bergerson, M. Bitter, D.L. Brower, E. Fredrickson, C. Gao, M. Greenwald, K. Hill, A. Hubbard, J. Irby, J.W. Hughes, E. Marmar, N. Pablant, S. Scott, R. Wilson, S. Wolfe, S. Wukitch, On the formation and stability of long-lived impurity-ion snakes in Alcator C-Mod, Nuclear Fusion, 53 (2013) 043019.

[38] R.D. Gill, A.W. Edwards, D. Pasini, A. Weller, Snake-like density perturbations in JET, Nuclear Fusion, 32 (1992) 723-735.

[39] D. Biskamp, Nonlinear Theory of the $m=1$ Mode in Hot Tokamak Plasmas, Physical Review Letters, 46 (1981) 1522-1525.

[40] Q. Yu, S. Günter, K. Lackner, Numerical modelling of sawtooth crash using two-fluid equations, Nuclear Fusion, 55 (2015) 113008.

[41] M. Ottaviani, F. Porcelli, D. Grasso, Multiple States of Nonlinear Drift-Tearing Islands, Physical Review Letters, 93 (2004) 075001.

[42] M.S. Chu, V.S. Chan, P.A. Politzer, D.P. Brennan, M. Choi, L.L. Lao, H.E.S. John, A.D. Turnbull, Kinetic Alfvén wave and associated current drive at the center of tokamaks, Physics of Plasmas, 13 (2006) 114501.

[43] M.S. Chu, D.P. Brennan, V.S. Chan, M. Choi, R.J. Jayakumar, L.L. Lao, R. Nazikian, P.A. Politzer, H.E.S. John, A.D. Turnbull, M.A.V. Zeeland, R. White, Maintaining the quasi-steady state central current

density profile in hybrid discharges, Nuclear Fusion, 47 (2007) 434-442.

[44] I. Krebs, S.C. Jardin, S. Günter, K. Lackner, M. Hoelzl, E. Strumberger, N. Ferraro, Magnetic flux pumping in 3D nonlinear magnetohydrodynamic simulations, Physics of Plasmas, 24 (2017) 102511.

[45] W. Zhang, Z.W. Ma, S. Wang, Hall effect on tearing mode instabilities in tokamak, Physics of Plasmas, 24 (2017) 102510.

[46] H.W. Zhang, J. Zhu, Z.W. Ma, G.Y. Kan, X. Wang, W. Zhang, Acceleration of three-dimensional Tokamak magnetohydrodynamical code with graphics processing unit and OpenACC heterogeneous parallel programming, International Journal of Computational Fluid Dynamics, 33 (2019) 393-406.

[47] L. Duan, X. Wang, X. Zhong, A high-order cut-cell method for numerical simulation of hypersonic boundary-layer instability with surface roughness, Journal of Computational Physics, 229 (2010) 7207-7237.

[48] C. Cheng, M. Chance, NOVA: A nonvariational code for solving the MHD stability of axisymmetric toroidal plasmas, Journal of Computational Physics, 71 (1987) 124-146.

[49] A.Y. Aydemir, J.C. Wiley, D.W. Ross, Toroidal studies of sawtooth oscillations in tokamaks, Physics of Fluids B: Plasma Physics, 1 (1989) 774-787.

[50] A.C.C. Sips, R. Arslanbekov, C. Atanasiu, W. Becker, G. Becker, K. Behler, K. Behringer, A. Bergmann, R. Bilato, D. Bolshukhin, K. Borrass, B. Braams, M. Brambilla, F. Braun, A. Buhler, G. Conway, D. Coster, R. Drube, R. Dux, S. Egorov, T. Eich, K. Engelhardt, H.U. Fahrbach, U. Fantz, H. Faugel, M. Foley, K.B. Fournier, P. Franzen, J.C. Fuchs, J. Gafert, G. Gantenbein, O. Gehre, A. Geier, J. Gernhardt, O. Gruber, A. Gude, S. G nter, G. Haas, D. Hartmann, B. Heger, B. Heinemann, A. Herrmann, J. Hobirk, F. Hofmeister, H. Hohen cker, L. Horton, V. Igochine, D. Jacobi, M. Jakobi, F. Jenko, A. Kallenbach, O. Kardaun, M. Kaufmann, A. Keller, A. Kendl, J.W. Kim, K. Kirov, R. Kochergov, H. Kollotzek, W. Kraus, K. Krieger, B. Kurzan, P.T. Lang, P. Lauber, M. Laux, F. Leuterer, A. Lohs, A. Lorenz, C. Maggi, H. Maier, K. Mank, M.E. Manso, M. Maraschek, K.F. Mast, P. McCarthy, D. Meisel, H. Meister, F. Meo, R. Merkel, D. Merkl, V. Mertens, F. Monaco, A. M ck, H.W. M ller, M. M nich, H. Murmann, Y.S. Na, G. Neu, R. Neu, J. Neuhauser, J.M. Noterdaeme, I. Nunes, G. Pautasso, A.G. Peeters, G. Pereverzev, S. Pinches, E. Poli, M. Proschek, R. Pugno, E. Quigley, G. Raupp, T. Ribeiro, R. Riedl, S. Riondato, V. Rohde, J. Roth, F. Ryter, S. Saarelma, W. Sandmann, S. Schade, H.B. Schilling, W. Schneider, G. Schramm, S. Schweizer, B. Scott, U. Seidel, F. Serra, S. Sesnic, C. Sihler, A. Silva, E. Speth, A. St bler, K.H. Steuer, J. Stober, B. Streibl, E. Strumberger, W. Suttrop, A. Tabasso, A. Tanga, G. Tardini, C. Tichmann, W. Treutterer, M. Troppmann, P. Varela, O. Vollmer, D. Wagner, U. Wenzel, F. Wesner, R. Wolf, E. Wolfrum, E. W rsching, Q. Yu, D. Zasche, T. Zehetbauer, H.P. Zehrfeld, H. Zohm, Steady state advanced scenarios at ASDEX Upgrade, Plasma Physics and Controlled Fusion, 44 (2002) B69-B83.

[51] N. Oyama, A. Isayama, G. Matsunaga, T. Suzuki, H. Takenaga, Y. Sakamoto, T. Nakano, Y. Kamada, S. Ide, Long-pulse hybrid scenario development in JT-60U, Nuclear Fusion, 49 (2009) 065026.

[52] I.T. Chapman, M.D. Hua, S.D. Pinches, R.J. Akers, A.R. Field, J.P. Graves, R.J. Hastie, C.A. Michael, Saturated ideal modes in advanced tokamak regimes in MAST, Nuclear Fusion, 50 (2010) 045007.

[53] W.A. Cooper, J.P. Graves, A. Pochelon, O. Sauter, L. Villard, Tokamak Magnetohydrodynamic Equilibrium States with Axisymmetric Boundary and a 3D Helical Core, Physical Review Letters, 105 (2010) 035003.

[54] J.A. Breslau, M.S. Chance, J. Chen, G.Y. Fu, S. Gerhardt, N. Gorelenkov, S.C. Jardin, J. Manickam, Onset and saturation of a non-resonant internal mode in NSTX and implications for AT modes in ITAB, Nuclear Fusion, 51 (2011) 063027.

[55] P. Buratti, M. Baruzzo, R.J. Buttery, C.D. Challis, I.T. Chapman, F. Crisanti, L. Figini, M. Gryaznevich,

T.C. Hender, D.F. Howell, H. Han, F. Imbeaux, E. Joffrin, J. Hobirk, O.J. Kwon, X. Litaudon, J. Mailloux, J.-E. contributors, Kink instabilities in high-beta JET advanced scenarios, Nuclear Fusion, 52 (2012) 023006.